JOURNAL OF GEOPHYSICAL RESEARCH, VOL. 106, NO. C11, PAGES 27,047–27,060, NOVEMBER 15, 2001

Measuring the shallow porosity structure of sediments on the continental shelf: A comparison of an electromagnetic approach with cores and acoustic backscatter

Rob. L. Evans
Department of Geology and Geophysics, Woods Hole Oceanographic Institution, Woods Hole, Massachusetts, USA

Abstract. We validate estimates of shallow sedimentary porosities made on the continental shelf by electromagnetic methods through a comparison with those measured directly in cores. Specifically, we show that an electromagnetic surveying system we have used to measure sediment resistivity in a number of seafloor locations returns porosity depth profiles that are related to those measured in cores, and that our data have good sensitivity to the structure within the uppermost few tens of centimeters of seafloor. We then consider inferences of sediment type made by observations of acoustic backscatter in the light of our porosity measurements. Our results suggest that electromagnetic methods provide complementary information that can be used to improve grain type estimates at and just below the seafloor, especially when combined with acoustic backscatter data. Because the system is pulled along the seafloor, data can be quickly collected from a large area of seafloor and can be used to interpolate facies conditions between core locations.

1. Introduction

The development of reliable seafloor surveying tools has made the use of electrical resistivity a viable geophysical approach for studying sedimentary processes on the continental shelf. Within seafloor sediments, the electrical resistivity is controlled by the amount and distribution of seawater, and so provides a useful handle on porosity. To first order, the empirical Archie's relationship [*Archie,* 1942], given by

$$\rho_m = \rho_f \phi^{-m},$$

provides a useful conversion between porosity (ϕ) and the measured resistivity (ρ_m), for a fairly narrow range of exponents m, and assuming a seawater conductivity (ρ_f).

Two large electromagnetic (EM) data sets have been collected in different sedimentary environments, one off California and the other off New Jersey [*Evans et al.,* 1999, 2000]. The data were collected using a towed EM surveying system owned and operated by the Geological Survey of Canada [*Cheesman et al.,* 1993; *Evans et al.,* 1999]. The system uses frequency domain magnetic fields to measure the electrical resistivity of the uppermost 20 m or so of the seafloor. The system consists of a large coil, which generates magnetic fields over a range of frequencies, and three receivers, which measure the amplitude and phase of these fields after propagation through the seafloor. The system is towed along the seafloor at speeds of 1-2 knots (1.8-3.7 km h^{-1}) and makes a measurement of seafloor resistivity every 10 m or so along track. The receivers are spaced 4 m, 13 m, and 40 m behind the transmitter and provide information at different depth intervals, generally to about one-half the source-receiver separation. Each receiver measures amplitude and phase at three frequencies, chosen so that the source-receiver separation is greater than a skin depth in the ocean (a skin depth is the length over which fields decay to $1/e$ of their original value). Since higher-frequency fields decay more rapidly, the 4 m receiver measures frequencies of 20 kHz to 200 kHz, while the 40 m receiver measures lower frequencies from 200 Hz to 2 kHz. In this paper we focus on the data provided by the 4 m receiver and demonstrate how these data (three amplitudes and three phases) average structure with depth. These six pieces of information are combined into an apparent resistivity (the resistivity of the uniform seafloor half-space best representing the data) and then into an apparent porosity using Archie's law given above. Below, we will refer to the apparent porosity derived from EM data as ϕ_a. These apparent porosity values provide a quick and convenient means of displaying raw field data for each of the three receivers.

Both survey areas from which we present data were targeted by the Office of Naval Research as focus ar-

Paper number 2000JC000487.
0148-0227/01/2000JC000487$09.00

eas for the STRATAFORM initiative [*Nittrouer and Kravitz,* 1996; *Nittrouer,* 1999]. Because of this initiative, there is a wealth of additional and coincident data in both regions, allowing us to perform this detailed comparison of EM and other techniques, such as coring [*Borgeld et al.,* 1999; *Sommerfield and Nittrouer,* 1999], side-scan sonar, and high-resolution bathymetric mapping [*Goff et al.,* 1999a, 1999b, 2000; *Mayer et al.,* 1996]. Most of the details of the EM data described in earlier publications focused on the deeper structure, to depths up to 20 m below the seafloor. In many cases, the uppermost few tens of centimeters of sediment are of great interest, as they offer insight into the most recent episodes of deposition, reworking, and, hence, modes of sediment transport. If the EM technique we discuss is to shed light on these processes, then it must have sufficient resolution over this shallow depth interval and should correlate with other sampling and imaging techniques.

The shallowest measure of resistivity is made by the 4 m receiver and provides information over the uppermost 2 m or so of the seafloor. We first demonstrate the resolution of data measured on this receiver through sensitivity analysis and the inversion of synthetic data. We use these results to construct a weighting function which quantifies how the system averages shallow structure. We next show the results of inverting field data and compare resistivity profiles with those predicted from core samples taken nearby. All of these steps demonstrate that the system has good shallow resolution and is able to identify high-porosity regions forming the uppermost few tens of centimeters of seafloor.

Given that our data have sufficient shallow resolution, we investigate the overlap between structure inferred from our resistivity measurements and that inferred from acoustic backscatter, a technique commonly used for seafloor classification. We show examples where the EM data show broadly correlated behavior with acoustic backscatter amplitude and identify a porosity signature associated with features seen in side-scan imagery. However, we also show examples where more complicated behavior is observed and discuss the mechanisms that might be responsible.

1.1. Survey Area 1: Eel River Shelf

The continental shelf near the Eel River, northern California, has undergone many surveys of geological structure. These surveys have defined the preserved strata, the local oceanographic environment, and the near-surface transport processes which control the ongoing construction of the shelf [*Nittrouer,* 1999]. The regional geology is dominated by tectonic activity associated with subduction of Gorda Plate and the northward migration of the Mendocino triple junction [*Clarke,* 1992; *Field et al.,* 1987]. High-resolution side-scan imaging identified features that are controlled by the local ocean currents, as well as by regional tectonics [*Goff et al.,* 1999a]. In general, the shelf is flat and featureless, particularly its inner regions, due to terrigenous input that derives from the Eel River to the south and the Mad River to the north. However, the shelf bathymetry contains a vertical bulge associated with recent flood input [*Goff et al.,* 1999a; *Wheatcroft et al.,* 1997]. The shallow resistivity structure on the Eel River shelf was seen to be highly variable, and three distinct environments were identified based on the recorded resistivities and the porosities inferred from them [*Evans et al.,* 1999] (Figure 1). The first region is a midshelf depocenter, characterized by a thin (~2 m), moderately high porosity (45-60%) surface layer which overlies a less porous (35-45%) and homogeneous substrate, uniform both laterally and vertically, and roughly coincident with recent flood deposits [*Wheatcroft et al.,* 1997]. The second region contains extremely high resistivities for a shallow sedimentary environment and has a high degree of spatial variability on length scales of several hundred meters. The third region roughly coincides with the Eel River subaqueous delta and features a buried layer of moderately low porosity (30-35%) at a depth of about 5 m and a thickness of between 5 and 10 m. Extensive coring and sampling have been carried out, allowing us to ground truth the EM data at a number of locations. High-resolution bathymetry and acoustic side-scan imagery have also been collected [*Goff et al.,* 1999a]. A comparison of acoustic backscatter amplitude (made by insonification at 100 kHz) versus grain size derived from box cores has been made [*Borgeld et al.,* 1999]. An outstanding issue is that the fine-grained sands that form the uppermost surface of the subaqueous delta have the lowest acoustic backscatter seen on the shelf, albeit by a fairly small margin of a few decibels. Counterintuitively, the high-porosity muds associated with the recent flood deposits show the highest backscatter intensities. X radiographs taken on the flood deposit show lenticular bedding, which *Borgeld et al.* [1999] claimed is responsible for enhancing acoustic returns.

1.2. Survey Area 2: New Jersey

Sedimentary input onto the New Jersey margin has been limited since the last major period of deglaciation [*Emery and Uchupi,* 1984; *Milliman et al.,* 1990]. In addition, the sequence of exposure and burial associated with glacial activity has resulted in complex patterns of sedimentary structures, both with depth and laterally across the margin. Much of the surface morphology reflects a substantial amount of reworking by ocean currents, but also contains long-wavelength sand ridge structures that were probably formed in a nearshore environment. The New Jersey EM survey primarily focused on a series of buried paleochannels that had been imaged through two- and three-dimensional (2-D and 3-D) seismic reflection profiling [*Davies et al.,* 1992; *Austin et al.,* 1996; *Davies and Austin,* 1997]. We completed a series of detailed survey lines across two areas

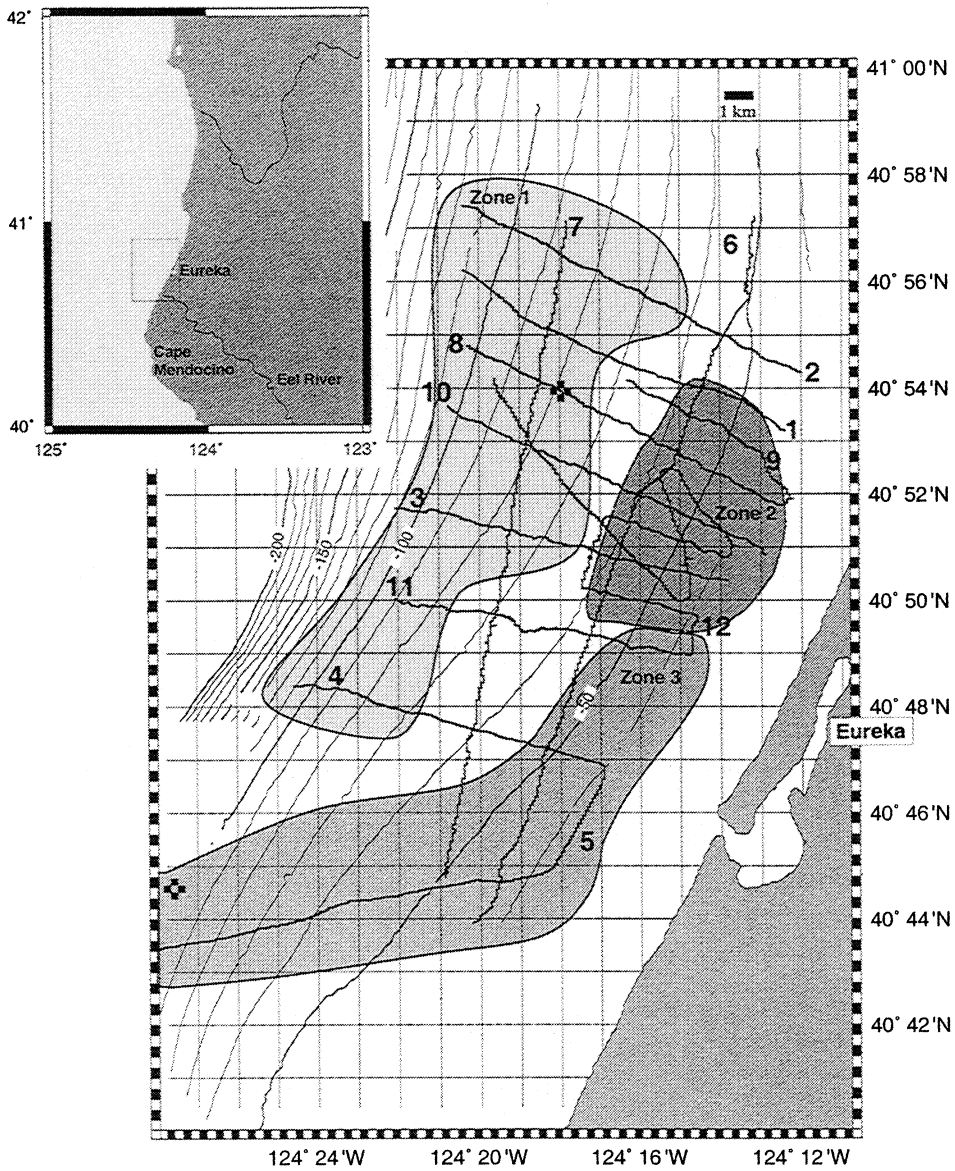

Figure 1. A map of the Eel Shelf survey area, off California, showing the 12 lines completed with the towed EM system. The data delineate three regions of distinct porosity structure labeled zones 1, 2 and 3, which are described in the text. Reprinted from *Evans et al.*, [1999], Copyright (1999), with permission from Elsevier Science.

that had featured 3-D seismic profiling and were able to identify the electrical signature of some of the buried paleochannels [*Evans et al.*, 2000] (Figure 2).

An unconformity found across much of the shelf is seen as a bright seismic reflector (named R) and represents a period when the shelf may have been subaerially exposed [*Milliman et al.*, 1990]. Regional Huntec surveying shows substantial variation in sediment thickness on top of R. Two prominent regions of post-R deposition are the midshelf and outer shelf sediment wedges described by *Milliman et al.* [1990]. These wedges lie on top of R and have thicknesses of up to 50 m on the outermost shelf and in excess of 15 m in midshelf. The two wedges are separated by a region where R outcrops at the seafloor or is covered by at most a veneer of sands. The midshelf wedge lies between 40 and 60 m water depth. The wedge itself is divided into two depocenters separated by the Hudson divide. The outer shelf wedge lies in water depths between 65 and 100 m at its southern end and trends northeast, increasing in depth as it approaches and overlies the Hudson apron. *Milliman et al.* [1990] suggested a nearshore deltaic setting for the deposition for these sediments. The substantial thickness of the wedge, in places 50 m thick, further suggests a rapid deposition. On top of these sediments lie a series of sand ridge deposits, oblique to mapped paleoshorelines and ribbon floored swales, which are bathymetric lows parallel to modern shelf currents [*Goff et al.*,

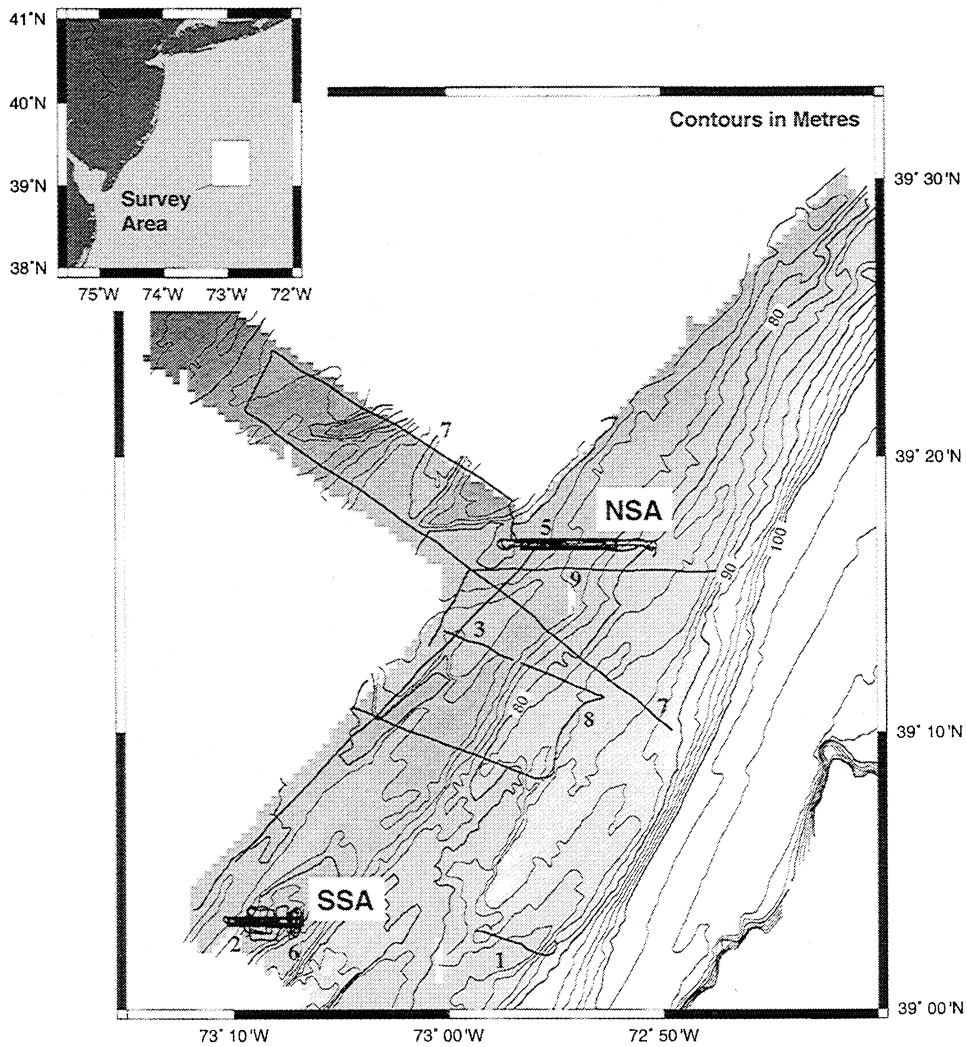

Figure 2. A bathymetric map of the New Jersey survey region [*Mayer et al.,* 1996; *Goff et al.,* 1999b] showing all the lines completed during the cruise. The two regions of dense coverage (labeled as the NSA and SSA [*Evans et al.,* 2000]) were the focus of previous 3-D high-resolution seismic surveys with the Huntec seismic system [*Davies et al.,* 1992; *Davies and Austin,* 1997; *Austin et al.,* 1996]. Reprinted from *Evans et al.,* [2000], Copyright (2000), with permission from Elsevier Science.

1999b; *Duncan et al.,* 2000]. The ridges are large-scale features and have relief of 1-10 m, widths of around 1-5 km, and along-strike lengths of tens of kilometers. Ribbons are smaller features, with submeter amplitude and spacings less than 200 m [*Duncan et al.,* 2000; *Goff et al.,* 2000].

Lines were run across regions that were covered by the outer shelf sediment wedge, as well as regions where R outcrops on the seafloor. Lines were also run over several midshelf sand ridges. While the sandy constituency of the sediments here has made coring difficult, there are some coincident grab samples, composite cores, and acoustic backscatter data from this region [*Goff et al.,* 1999b, 2000].

2. Shallow Sensitivity of the EM System

In this section, we will use three separate approaches to demonstrate the shallow resolution of EM data collected with the towed EM system in its present configuration. The most straightforward means of estimating the sensitivity of the system to shallow structure is through perturbation of a representative porosity profile, and comparison of the synthetic responses for the perturbed and starting model. Formally, this perturbation would be computed by Fréchet derivatives for the particular system [*Chave,* 1984]. We have chosen to carry out a numerical calculation of sensitivity. In doing so, we define the "response", $F[\rho(z)]$, at a given receiver to consist of the six amplitude and phase values

recorded (i.e., one amplitude and phase value for each of the three received frequencies), where $\rho(z)$ is the resistivity as a function of depth below the seafloor, z. Therefore a change in response will be a summation of the changes in each amplitude and phase referenced to those of the original model. Details of the calculation of the forward response of a coaxial vertical magnetic dipole source and receiver, appropriate for the towed EM system used, is given by *Cheesman et al.* [1987]. The calculation involves the numerical integration of Bessel functions as described by *Chave* [1983]. The interested reader will find further details on the theory and practice of marine electromagnetic methods in the works by *Chave and Cox* [1982], *Chave et al.* [1987], and *Constable* [1990].

The most obvious representative profile for perturbation analysis is a uniform half-space model. We have therefore calculated the predicted change in data recorded on the 4 m receiver that results from perturbing a uniform half-space model, discretized into layers 5 cm thick, at each layer in turn. We perturb the ith layer by 0.1% of its original resistivity. Under normal circumstances, we would have to carry out this perturbation in the log domain, as resistivity through a typical Earth model can vary by several orders of magnitude. In seafloor sediments, and especially near the seafloor, the ranges in resistivity expected are considerably smaller than we might normally encounter. For example, seawater has a resistivity of 0.28 Ω m at temperatures typical of bottom water. A sandy sediment with a porosity of 40% is predicted by Archie's law to have a resistivity of 1.45 Ω m, or 5 times that of seawater. This is probably the most extreme case we will have to deal with: averages of cores from the Eel River shelf generally show porosities in excess of 50%. Therefore we consider a linear perturbation to be sufficient, and we calculate the change in amplitude and phase values for all three frequencies on a receiver caused by this change in resistivity. We evaluate the sum of these changes for each layer, j, as

$$\frac{\delta F[\rho(z)]}{\delta \rho} \approx \frac{\Delta F_j}{\Delta \rho_j} = \sum_{i=1}^{3} \{\Delta A(\omega_i, j)/\Delta\rho_j + \Delta\Psi(\omega_i, j)/\Delta\rho_j\},$$

where ρ_j is the jth layer in a discretized model of resistivity versus depth $\rho(z)$. $A(\omega_i, j)$ is the amplitude of the received magnetic field at frequency ω_i, and $\Psi(\omega_i, j)$ is the corresponding magnetic field phase. Each receiver records amplitude and phase information at three frequencies.

We normalize the changes at each layer by the maximum observed change over the whole model. A sensitivity curve for a uniform 1 Ω m half-space is shown in Figure 3. The peak in sensitivity occurs near the seafloor and falls off essentially to zero by about 2.5 m depth.

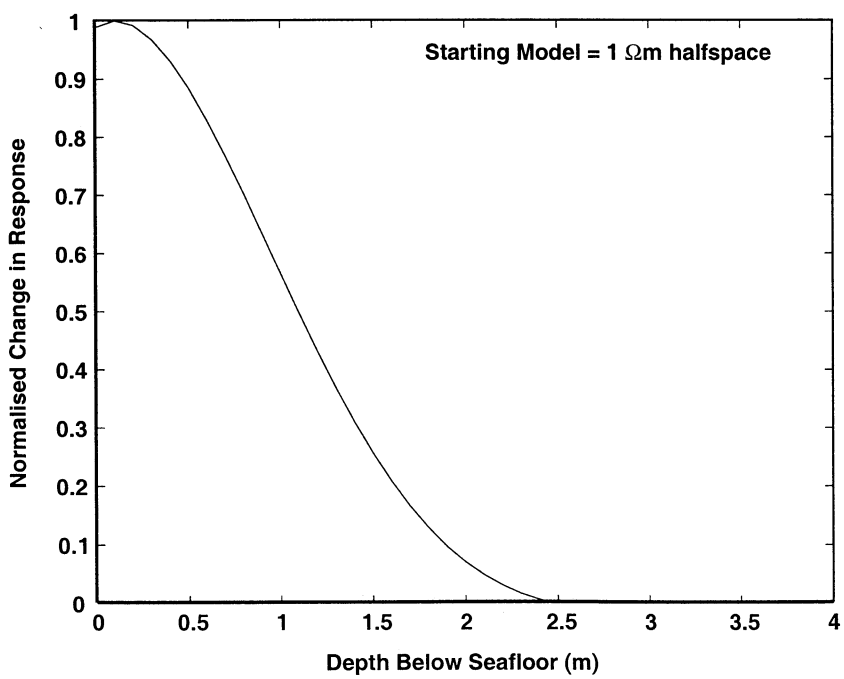

Figure 3. Sensitivity curve for the 4 m receiver calculated by perturbing a multilayered but uniform model of 1 Ω m. The peak in sensitivity is immediately below the seafloor and falls essentially to zero at a depth of 2.5 m.

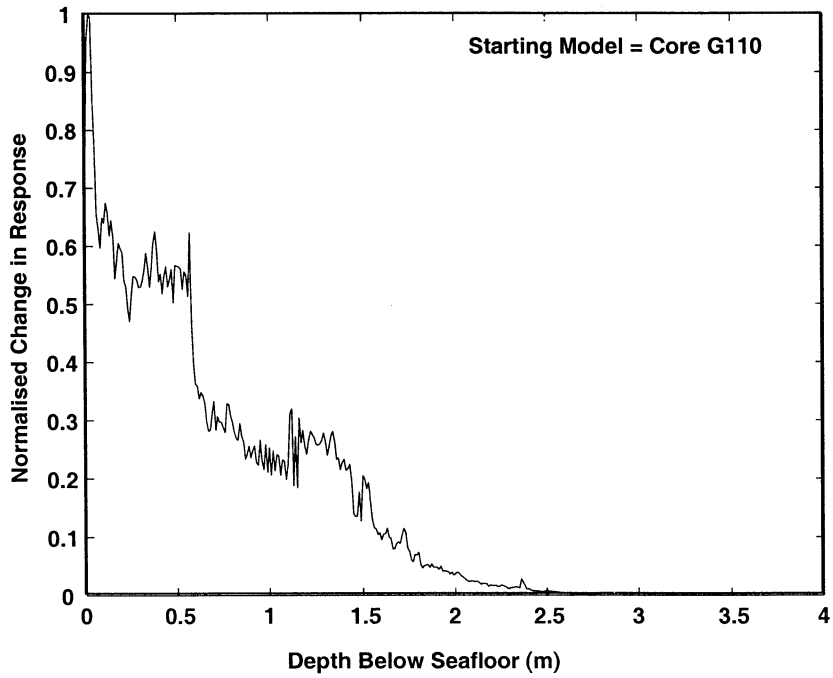

Figure 4. Sensitivity curve using the G110 core profile as a starting model. In this case, the falloff in sensitivity with depth is more rapid, but approaches zero at the same 2.5 m depth.

2.1. Cores and Apparent Porosity, ϕ_a

A series of cores have been collected across the Eel shelf [*Sommerfield and Nittrouer,* 1999], and we use these to examine the effect on our data of more realistic variations in porosity. The cores have been logged using a multisensor track system measuring, among other parameters, gamma ray attenuation, which provides a proxy for density of sediment and, hence, porosity [*Kayen and Thang,* 1997; *Kayen et al.,* 1999].

We have used one of these core profiles (G110) as a basis for modeling resistivity structure. The core was collected on the outer shelf off California and was chosen because it has variability and discrete units within it. A large spike in the original core, probably the result of gas expansion, has been removed to construct the profile we use.

Porosity measurements were made at 1 cm intervals and were converted to resistivity using Archie's law with an exponent of 1.8. We performed the same perturbation calculation as for the half-space, and the results are shown in Figure 4. Once again, the peak in sensitivity occurs near the seafloor, and sensitivity reaches zero around a depth of 2.5 m, but in this case falls off faster with depth.

We have used the sensitivity curve for the uniform half-space to construct a weighting function from which we calculate an average porosity $< \phi >$ from the observed core profiles:

$$[\delta F]^* = \int_0^\infty \frac{\delta F[\rho(z)]}{\delta \rho(z)} dz \approx \sum_{j=1}^{N} \frac{\Delta F[\rho]_j}{\Delta \rho_j} dz_j,$$

$$< \phi > = \frac{1}{[\delta F]^*} \int_0^\infty \phi(z) \frac{\delta F[\rho(z)]}{\delta \rho(z)} dz \approx \frac{1}{[\delta F]^*} \sum_{j=1}^{N} \phi(j) \frac{\Delta F[\rho]_j}{\Delta \rho_j} dz_j,$$

where $z_N \gg 2.5$ m, or the depth at which the data lose sensitivity.

We have also calculated the best fitting apparent porosity to synthetic responses for each core profile. The values obtained through both methods agree to within 1% porosity.

We show values of apparent porosity measured with the EM system versus those predicted from core profiles using the depth-averaging function described above (Table 1). Only a few of the cores are within 100 m of the nearest EM measurement, but even so the agreement between the two estimates is within a few percent.

2.2. Inversion of Synthetic Data: Shallow Resolution

By calculating an apparent porosity, we are essentially throwing away information contained in the data. It is possible to use all the amplitude and phase data from all receivers as independent constraints and invert for resistivity as a function of depth. However, while this process returns more information than simple half-space values, the EM method will, in general, be unable to resolve thin layers of anomalous resistivity. The computations involved in carrying out these inversions are sufficiently complex that they preclude inverting entire profiles of data. Instead, our approach has been to invert data at a few well-chosen locations,

Table 1. A Comparison of Apparent Porosity ϕ_a Measured on the 4 m Receiver with the Closest Available Core Profile[a].

Core	Distance (m)	ϕ_a	$<\phi>$
G110	25	50.72	52.0
O70	168	52.90	55.7
S80	93	53.00	57.2
S90	110	54.61	56.5
S100	307	54.45	53.3
T110	410	56.26	59.5

[a]The average porosity for the core, $<\phi>$, was calculated using the weighting function described in the text. The "distance" column refers to the separation of the EM system and the core station at the point of closest approach. Core data are courtesy of C. Sommerfield and Homa Lee.

normally where responses are as one-dimensional (little variation between adjacent measurements) as possible, and use apparent porosity information to interpret between these inverted profiles.

We have generated synthetic data using the same core (G110) as previously. We invert these data for a maximally smooth resistivity depth model, that is, a model that has the least amount of structure required to fit the data to a specified tolerance. Because the core profiles extend deeper than the 2.5 m at which the 4 m receiver loses resolution, we have included the two highest frequencies from the 13 m receiver in the subsequent analysis. The Occam algorithm [*Constable et al.*, 1987] minimizes the roughness of the model while satisfying the target misfit. A featureless or smooth model will have a minimum integrated roughness over its length, where roughness can be defined as

$$R_1 = \int_0^\infty \left(\frac{d\rho}{dz}\right)^2 dz,$$

$$R_2 = \int_0^\infty \left(\frac{d^2\rho}{dz^2}\right)^2 dz.$$

R_1 is the measure of roughness with respect to the first model derivative, and penalizing this measure results in the flattest model possible, or the model closest to a uniform half-space. R_2 is the measure of roughness with respect to the second model derivative, and penalizing this returns the least oscillatory or "wiggly" model.

Under normal circumstances, with Gaussian errors in our field data, we should expect to fit the data to an RMS misfit of 1.0 (or a χ^2 misfit equal to the number of data). In general, the lower the target misfit, the more structure will be required in the data, and the rougher the resulting model. Not all of the observed increase in structure is meaningful. Suppose that the seafloor were a uniform half-space, but that the data measured contain deviations from a true half-space response due to experimental error. If we have good controls on the sizes of these errors, then we should be able to choose the appropriate level of misfit and the model returned would be the uniform half-space. As we lowered the misfit beneath the optimal level, the structure in the model would increase. The important thing to note is that only minor decreases in the target misfit can cause geologically significant changes in the resulting model. In practice, we determine error levels by towing the system through the water column and compare the estimate of seawater conductivity determined by the system with that measured by a conductivity-temperature-depth (CTD) unit at the front of the array. This means that we have a good determination of the noise within the system itself, but not of the effects of geometric changes in the array configuration on the bottom, for example, the effects of rough topography, or local three-dimensionality in resistivity structure.

With ideal synthetic data, we can perform inversions at steadily lower degrees of misfit and see how the structure in the model changes. Figure 5 shows models returned at misfit values of 2.0, 1.0, and 0.2.

The errors used to weight the misfit are the same as for our field data, but the calculated values have not been perturbed. The data were calculated using a 500 layer model at 1 cm thickness intervals. The inverse model has 99 layers logarithmically spaced with depth. Because of these different depth parameterizations a perfect match between model and data is not found, although in principle a zero misfit should be achievable. However, when inverting field data, we would not fit to less than 1.0 for fear of introducing spurious structure into the model not required by the data.

The model which fits to RMS 0.2 is essentially a low-pass filtered version of the starting model and contains a good representation of the shallowest portion of the core profile. Decreasing the misfit to 0.15 starts to introduce more oscillations into the model, and the linearized search algorithm starts to break down. A fit to 1.0 reproduces the bulk properties of the core profile, but does less well near the seafloor.

2.3. Inversion of Real Data

We have inverted data close to core S80, which contains a high-porosity layer extending from the seafloor to a depth of around 20 cm (Figure 6). A fit to RMS 1.7 shows excellent agreement between the models and the core profile, even at the seafloor. Once again, the inverse model is a low-pass filtered version of the core profile. Reducing the misfit further causes the inversion to become unstable and the models to become oscillatory. Not only does this result give us confidence in the resolution of the system, but it also is convincing that the transformation from resistivity to porosity is reliable, at least to first order.

There are several key points to note here. First of all, our apparent porosities represent a weighted average of the sediment porosity. Data on the 4 m receiver have a weighting function which peaks at the seafloor and

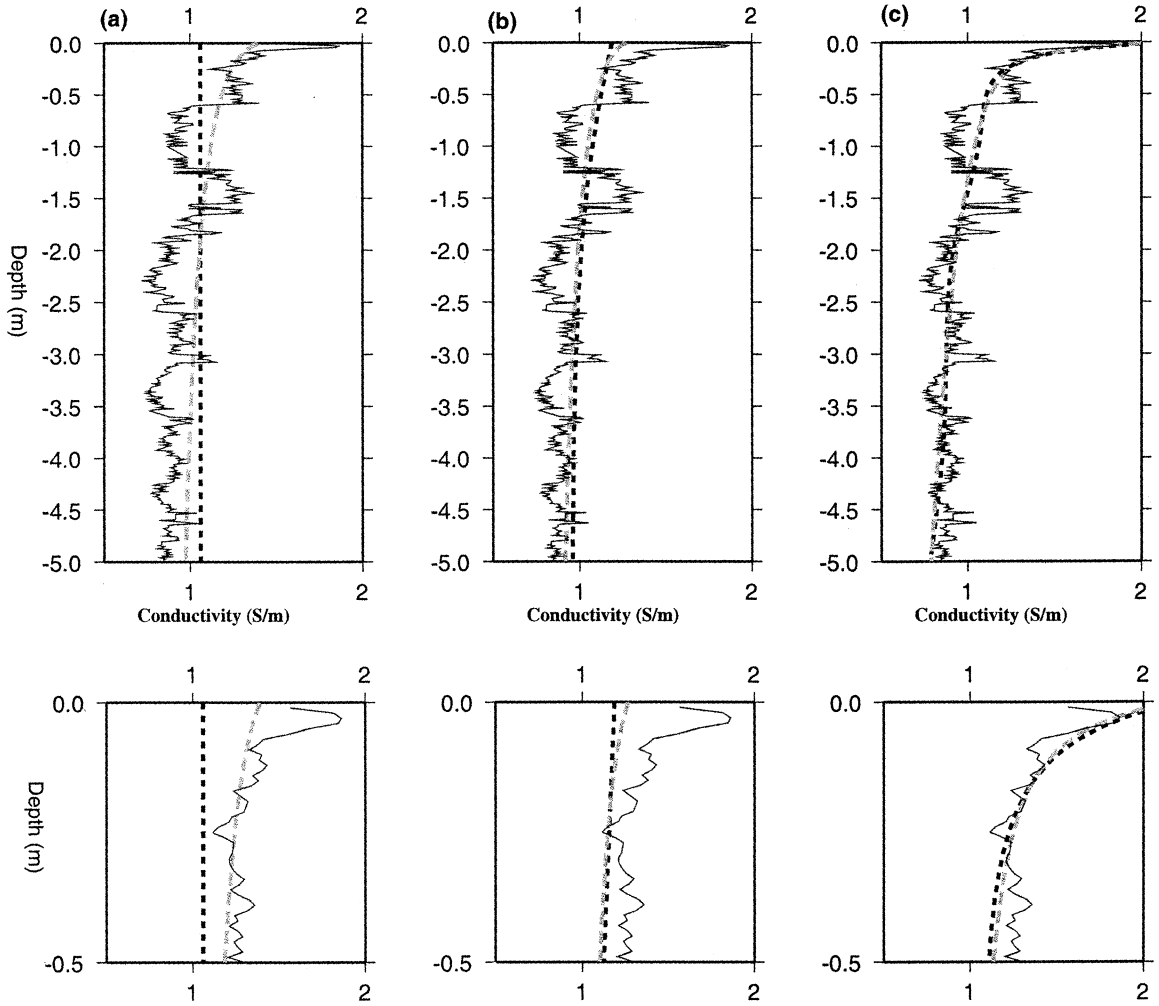

Figure 5. Inversions of synthetic data generated from the G110 core profile. The starting profile is shown in black in each figure. The achieved RMS misfit between the starting data and inverse model response is (a) 2.0, (b) 1.0, and (c) 0.2. The two models in each panel are optimally smooth with respect to their first (dark dashed line) and second (light dashed line) derivatives. The lower panels show a close-up view of the top 50 cm of core and model. The models which fit to RMS 0.2 are low-pass filtered versions of the starting model and show good agreement with the core profile close to the seafloor.

which diminishes around 2.5 m depth. Second, these apparent porosities show good agreement with weighted averages constructed from core profiles. Even though our data are unable to resolve details of thin layers, the nature of the weighting function does mean that we have sensitivity to structure within the first 10 cm of the seafloor. Finally, using data to invert for depth profiles of resistivity demonstrates that the information held by the data is equivalent to a low-pass filtered version of the true resistivity-depth profile.

3. Depths of Sensitivity of Side-Scan and EM Data: Do They Overlap?

The previous sections aimed to show that the towed EM system provides robust measures of sediment porosity and has resolving power within the uppermost few tens of centimeters of seafloor. It is intriguing, therefore, to examine whether there is any relationship between the shallow apparent porosities measured by the EM system and acoustic backscatter measured using side-scan sonar systems.

Acoustic backscatter has had widespread use as a means of classifying sediment type [e.g., *Goff et al.*, 2000; *Hughes-Clarke*, 1993; *Hughes-Clarke et al.*, 1996; *Jackson and Briggs*, 1992]. Correlations between backscatter amplitudes and grain type and size have been attempted, but it seems clear that the variety of scattering mechanisms make general inference of sediment properties from backscatter difficult. The primary scattering mechanisms are volume scattering from grains and heterogeneity within the uppermost sediment at the seafloor, and surface scattering, particularly from surface roughness [*Jackson and Briggs*, 1992].

For there to be overlap between EM and acoustic backscatter, there must be some overlap in the scale

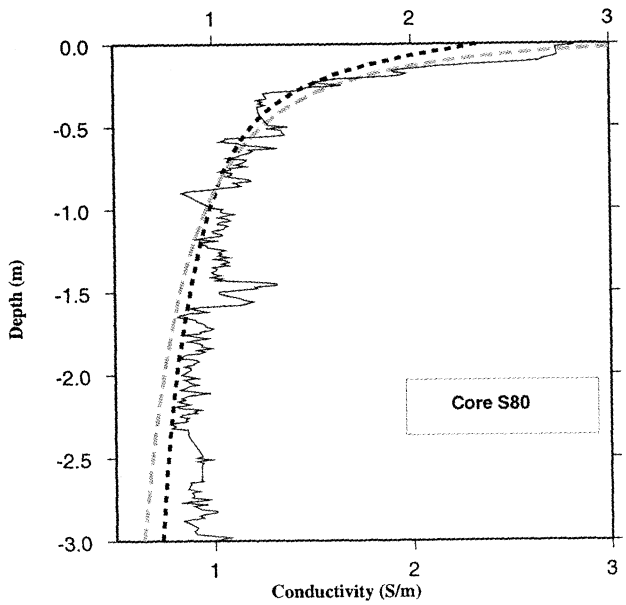

Figure 6. Inversion of real data collected on the seafloor approximately 90 m away from core S80. The two models are, again, optimally smooth with respect to their first (dark dashed line) and second (light dashed line) derivative. The misfit between the model response and the data is 1.7. Reducing the misfit further results in an oscillatory model.

over which the two systems sample the seafloor. We have shown that the EM system is sensitive to structure in the top 10 cm and returns some estimate of the bulk properties over that interval. Furthermore, our surveys have sampled a variety of sediment type. Side-scan operates at frequencies of around 100 kHz, or wavelengths of 1-2 cm. The depth to which acoustic energy penetrates the seafloor is controversial. Energy absorption calculations suggest that side-scan systems do not penetrate any deeper than about a wavelength into the seafloor, if even that far [*Mourad and Jackson,* 1989]. The presence of gas within the sediment will also have a dramatic impact of acoustic return, although there is no firm agreement quantifying this impact. There seems to be general agreement within the acoustic community that sands behave in a different manner to muds. It is beyond the scope of this paper to attempt an explanation for scattering behavior. However, it is unusual to have porosity and backscatter measurements made at a similar spatial density across such a large region of shelf, and so we present these data as a demonstration of the complexity of the problem and as a means of evaluating the extent to which porosity has a first-order control on acoustic backscatter.

4. Backscatter and Porosity Relationships: Sands Versus Muds

The link between sediment type and acoustic backscatter amplitude on the Eel shelf has already been seen by others to be problematic [e.g. *Borgeld et al.,* 1999; *Goff et al.,* 1999a]. The lowest observed backscatter amplitudes are seen in the Eel River subaqueous delta, a region of fine sands, while the highest amplitudes are seen from high-porosity, fine-grained muds that form the recent flood deposit. While this observation runs counter to most observations elsewhere [e.g. *Hughes-Clarke,* 1993; *Hughes-Clarke et al.,* 1996] the amplitude of the discrepancy is not large, only a few decibels. Furthermore, this is not the only place where muds have shown higher backscatter than fine sands [*Lyons and Abraham,* 1999]. *Borgeld et al.* [1999] compared porosity measurements from box cores with acoustic backscatter amplitude. They found a weak correlation between the two. Their data could be described as containing a population of high-porosity samples (57-75%) that do not show any change in amplitude as a function of porosity, and a set of samples ranging from 45% to 57% for which a 7 dB range in amplitude is seen, almost independent of porosity.

For both the Eel River and New Jersey regions, we have extracted side-scan backscatter amplitudes from the data collected by *Goff et al.* [1999a, 1999b] at points coincident with our EM data. A plot of acoustic backscatter versus apparent porosity (4 m) for our entire Eel River and New Jersey data sets does not appear to show any link between the two parameters (Plate 1). However, if subsets of the data are examined, both in plots of apparent porosity versus backscatter and through plots along profile, some of the links between the two responses can be seen. If we examine data collected approximately within the subaqueous delta, or zone 3 as defined by Evans et al. [1999], a negative correlation between backscatter and porosity appears (Plate 1, bottom). Data collected further north, away from the subaqueous delta, show a different behavior altogether. Acoustic backscatter and apparent porosity are shown along a profile from south to north, beginning at the northern limit of the Eel River subaqueous delta (Figure 7). For the first 12 km of the profile (-24 km to -12 km), backscatter amplitude and porosity appear to be closely related, with backscatter increasing with porosity. This is the reverse of the trend seen within the delta itself. Within this trend are a series of ribbon features, characterized by across-shelf regions of alternately high and low backscatter as reported by *Goff et al.* [1999a]. These ribbons are 0.2 to 1 km wide and are close to the sand-mud transition. Where this profile crosses these ribbon features (between -16 km and -20 km), peaks and troughs in backscatter correspond with local peaks and troughs in porosity. *Goff et al.* [1999a] interpreted these ribbons as downslope flow features with sand closer to shore being swept across the offshore muds. Data from New Jersey that are known to sample sands [*Buck et al.,* 1999] show an extension of the trend seen above, with lower porosities seen in the uppermost 1-2 m of seafloor. These data are from lines 2 and 5 of the survey [*Evans et al.,* 2000] which were across two regions containing buried paleochannels, on

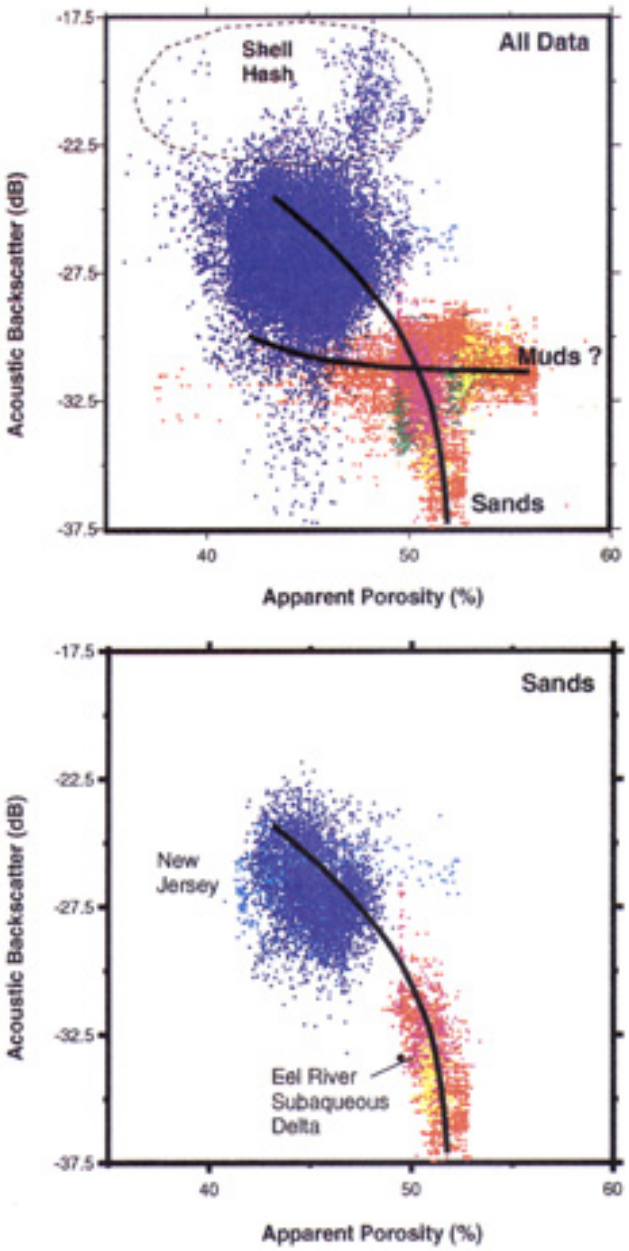

Plate 1. (top) Plots of acoustic backscatter amplitude versus apparent porosity for all of the data collected on both the Eel River shelf and the New Jersey margin (Blue colors). (bottom) A subset of the data from sandy environments is shown in the lower panel. This subset suggests that lower-porosity sands display higher acoustic backscatter. The top panel highlights the complexity of predicting backscatter from sediment type, once muds and shell hash are introduced.

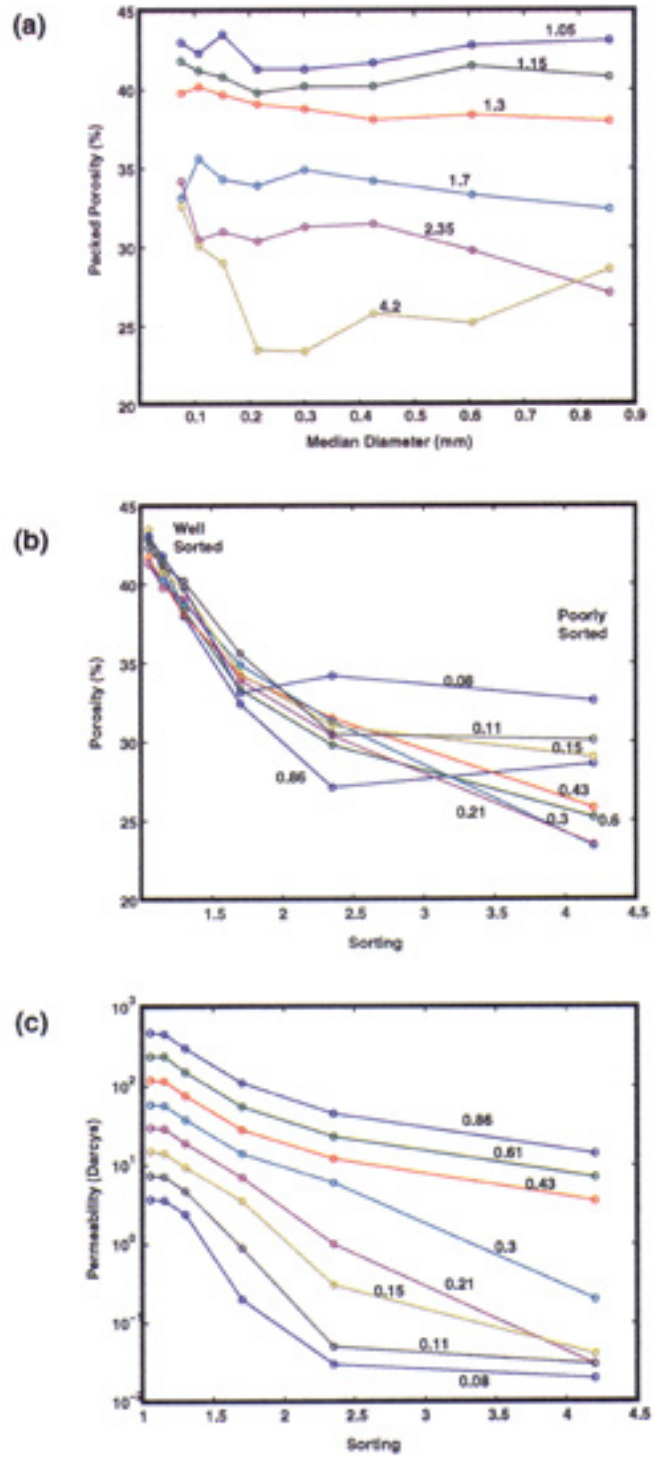

Plate 2. Porosity and permeability measurements as a function of sorting and median grain size from *Beard and Weyl* [1973]. The reader is directed to the original paper for full details of the data acquisition. All panels are for packed samples. (a) Porosity versus median grain size. The labels on each line are the degree of sorting (a larger value indicates poorer sorting). (b) Porosity as a function of sorting, with each line labeled by the median grain size. (c) Permeability versus sorting, with each line labeled with median grain size. Note that for a given grain size, at least an order of magnitude change in permeability is achievable by changing the degree of sorting.

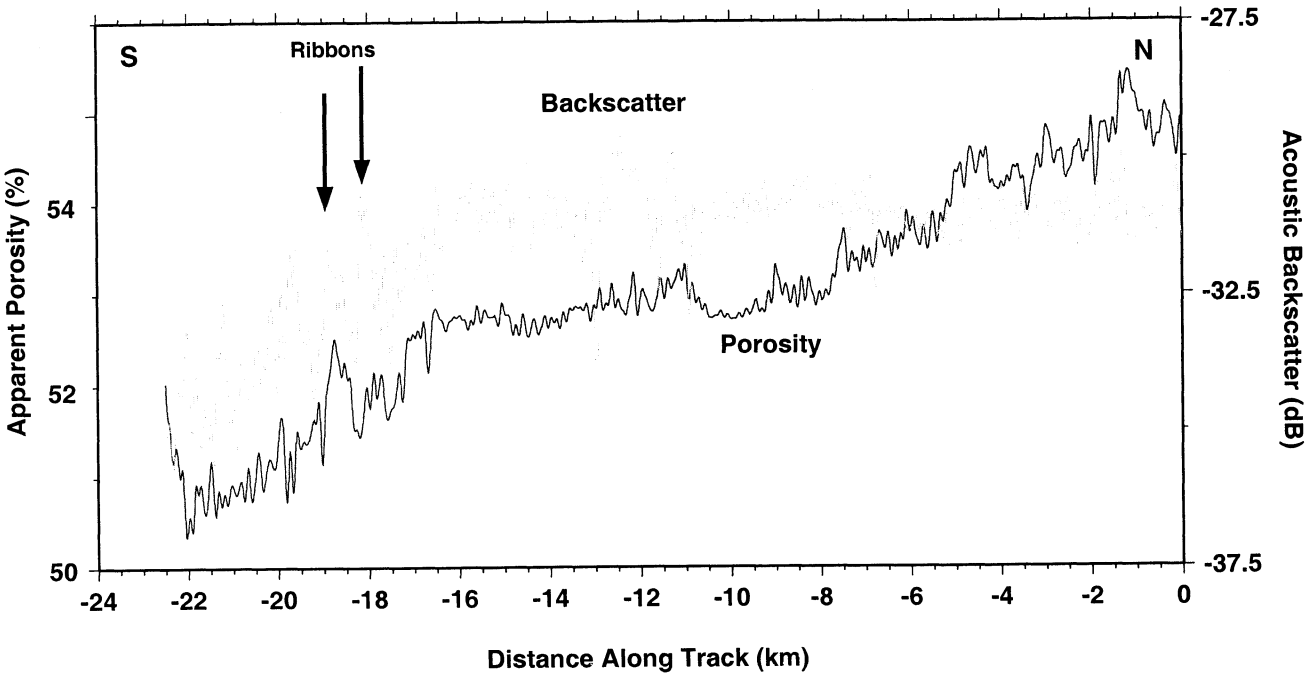

Figure 7. Track plots of apparent porosity and acoustic backscatter along a line (line 7) beginning at the northern end of the Eel River subaqueous delta and heading north. Features identified by *Goff et al.,* [1999a] as ribbons show a corresponding porosity signature. There is a general correlation between both data up to a distance of -8 km. Further north, in a region of high-porosity flood deposit muds, backscatter stays at an essentially constant level as porosity increases.

the western edge of an outer shelf wedge of sediment. The New Jersey data show greater variability, probably due to the effects of shell hash and occasional muds [*Goff et al.,* 1999b, 2000].

A different relationship between backscatter and porosity is seen on the Eel River shelf as the EM system crosses into the mud-dominated region of recent flood deposits. This change can be seen in the northernmost portion of the profile shown in Figure 7 (-12 km to 0 km). Here, as porosity continues to increase, backscatter levels remain essentially constant. The same trend holds true if data from zone 1 are examined in a porosity-backscatter plot.

We suggest that sands and muds have inherently different scattering mechanisms that result in two different relationships between porosity and acoustic backscatter. In sands, porosity is negatively correlated with backscatter. This is intuitive and is in broad agreement with other observations [e.g., *Hughes-Clarke et al.,* 1996]. Lower-porosity sands are more likely to be coarser grained and therefore more effective scatterers of 100 kHz acoustic energy. Surface roughness is also more likely to play a role in scattering from sands [*Jackson and Briggs,* 1992]. More difficult to explain is that the transition to muds, which increases porosity, also increases acoustic backscatter, although in mud-dominated strata backscatter reaches a limit beyond which it is essentially independent of porosity. Faced with the dilemma of apparently high backscatter amplitudes from muds compared to the sands in the Eel River subaqueous delta, *Borgeld et al.* [1999] suggested volume scattering from heterogeneity as a means of enhancing backscatter in the high-porosity muds.

On the basis of a set of backscatter data that show little relationship to bottom characteristics, *Lyons and Abraham* [1999] were forced to conclude that scattering strength is not an accurate descriptor of sediment type. They collected data from the Mediterranean in which a muddy station showed consistently higher backscatter amplitudes at grazing angles greater than 20° than a sandy site. Our data suggest that combining side-scan with widespread measures of porosity provided by EM surveying might allow a more definitive identification of sands and muds.

5. Sand Ridges on the New Jersey Margin

Measurements of apparent porosity crossing the axis of a large sand ridge on the New Jersey shelf show local minima in porosity (approximately 5% lower than the surroundings) at the position of local topographic highs or stationary points (Figure 8). Most studies of sediment properties across sand ridges show maxima in grain size on the upstream flank of the ridge [e.g., *Smith,* 1969; *Swift et al.,* 1978]. In order to understand how our data fit into this model, we need to understand the link between grain size and porosity. Given that abun-

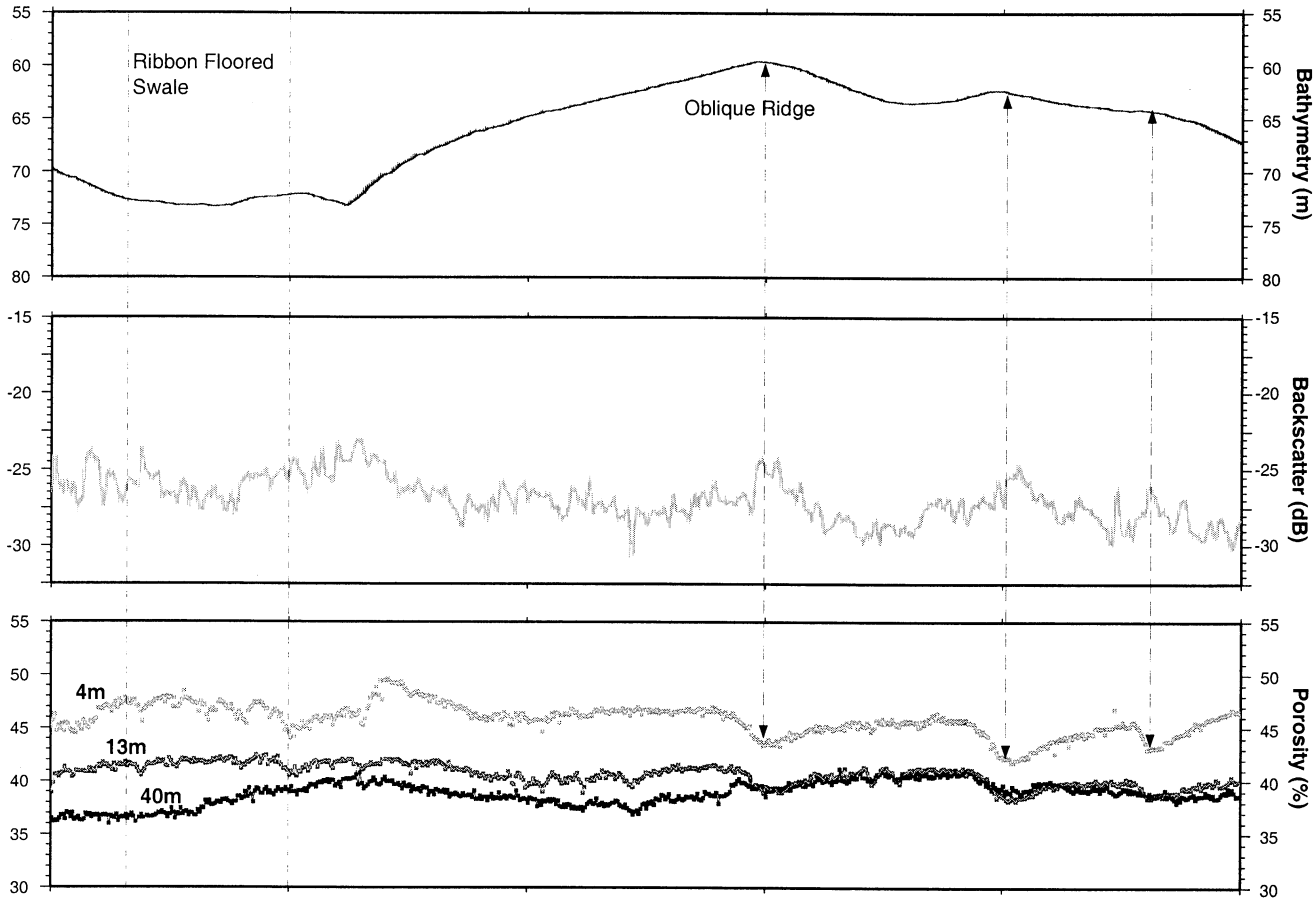

Figure 8. Porosity (derived from towed EM data), backscatter and bathymetry across a mid-shelf ridge on the New Jersey shelf. The EM data were collected along the north-eastern limb of line 7 of Figure 2. Across the ridge, local highs in topography appear as lows in the apparent porosity measured by the 4m receiver.

dant shell hash has been seen across these ridges, we will also need to understand the effects of nonsphericity in grain shape on resistivity.

The link between grain size and porosity is not straightforward. While it is intuitive to think of coarser grained sands as having low porosity (which is certainly true when compared to fine-grained muds), in reality, sorting plays a critical role in determining packing structure, and hence the porosity. In a classic study of the effects of texture on porosity and permeability *Beard and Weyl* [1973] showed how changes in median grain size had little effect on porosity or permeability. Their measurements of porosity and permeability as a function of sorting and grain size are shown in Plate 2. In particular, these data show that a poorly sorted sand with a coarse median grain size would have a similar (low) permeability to a well-sorted, fine-grained sand. In contrast, a well-sorted, coarse-grained sand showed a permeability 2 orders of magnitude higher. While the link between permeability and resistivity is tenuous, to first order and under saturated conditions, a more permeable sediment should have a lower resistivity. Some suggest that in sedimentary rocks permeability is proportional to the square of conductivity [e.g., *Wong et al.,* 1984].

We might expect the sediment on the upstream flank of the ridge to be coarser grained and well sorted, the finer-grained material having been winnowed away by currents. *Goff et al.,* [1999b] suggested that substantial winnowing has occurred across the midshelf ridges on the basis of grain size distributions across the ridges and elsewhere on the shelf. If the material on the top of the ridge has the same median grain size, but is less well sorted, it might have a lower porosity *Beard and Weyl,* [1973], which is what we see. The porosity of the down-stream flank will depend on whether the fine-grained material is dumped here, or whether it is transported out of the region. Side-scan data across the ridges are equivocal, but do seem to show modest peaks in backscatter amplitude coincident with the lows in porosity. Grain size distributions from grab samples across the ridges do not show any clear correlation with these observations [*Goff et al.,* 2000], although some of the samples contain large fragments of shell hash, which cause a dramatic enhancement in the acoustic backscatter returns.

Sphericity of grain shape has been shown to be a key factor in determining the exponent in Archie's law [*Jackson et al.,* 1978]. A possible explanation for the drop in apparent porosity is that it is in fact an increase in tortuosity caused by nonspherical, or platey shell fragments, and that we have misrepresented the porosity by using an inappropriate Archie exponent. *Jackson et al.* [1978, their Figure 9] showed a plot of Archie exponent m as a function of the percentage of shell fragments within a sediment sample. Exponent m increases from around 1.4 for a quartz sand to 1.9 as the percentage of shell fragments increased to 70%. For a given measured resistivity, a higher value of m predicts a higher porosity. We have used an exponent of 1.8 when calculating apparent porosities and when comparing the core profiles to resistivity profiles shown above. This value is appropriate for porosities in excess of 50%, as seen near the seafloor off California. It is plausible that a regional value of 1.4 would be more applicable for the sandy New Jersey shelf, locally increasing to 1.8 across the tops of the ridges as shell fraction increases. From Figure 8, the drop in porosity across the top of the ridge is 4%, from 47% on the inshore slope to 43% at the crest. If the appropriate exponent of m on the ridge flanks is 1.4, then these sediments would have a porosity of 38% instead of 47%, lower than at the topographic high. This is the extreme case. It is possible to imagine sediment grain size distributions across the ridge that result in an increase in resistivity with little or no change in porosity, but with a larger shell fraction at the peaks of the ridge.

6. Conclusions

Resistivity depth profiles obtained from EM surveying of continental shelf sediments provide an alternative and reliable means of mapping sediment properties. While the technique is not able to delineate thin layers of variable porosity, the system is able to identify high porosity deposits extending a few tens of centimeters into the seafloor and provides a low-pass filtered version of the shallow porosity structure. We have constructed a weighting function which describes how the system senses the shallowest porosity structure. We have shown the extent to which our data reproduce porosity profiles measured on cores. The profiling nature of the system makes it an attractive means of interpolating structure between core locations, providing facies information over greater areas of seafloor than is possible by coring alone.

We have demonstrated that the system has reasonable resolution near the seafloor, and that the shallowest apparent porosity is biased by the shallowest structure. This shallow resolution allows us to compare porosity estimates from our data with acoustic backscatter amplitudes. Others have suggested the difficulty of using acoustic backscatter as a sole determinant of sediment type: we suggest that porosity estimates from EM surveys might provide a useful additional constraint allowing more accurate sediment classification over large areas of seafloor. We caution, however, that ground truthing through cores or grab sampling at discrete locations remains important, as subtle changes in grain shape distributions can impact the porosity estimates derived from resistivity.

Acknowledgments. I would like to thank Chris Sommerfield and Homa Lee for kindly providing the core measurements. John Goff provided bathymetric and side-scan sonar data for both California and New Jersey regions. Ralph Stephen and Maurice Tivey are thanked for providing comments the paper. Associate Editor John Klinck and an anonymous reviewer are also thanked for their assistance. All aspects of this project were funded by the Office of Naval Research, through the office of Joe Kravitz, whose support is greatly appreciated. Data acquisition was funded by ONR grants N00014-96-1-0843 and N00014-98-1-0506. Further support for data analysis was provided by ONR grant N00014-98-1-0507. WHOI contribution number 10518.

References

Archie, G.E., The electrical resistivity log as an aid in determining some reservoir characteristics, *J. Pet. Technol., 5*, 1-8, 1942.

Austin, J.A., C.S. Fulthorpe, G.S. Mountain, D.L. Orange, and M.E. Field, Continental-margin seismic stratigraphy: Assessing the preservation potential of heterogeneous geologic processes operating on continental shelves and slopes, *Oceanography, 9*, 173-177, 1996.

Beard, D.C., and P.K. Weyl, Influence of texture on porosity and permeability of unconsolidated sand, *Am. Assoc. Pet. Geol. Bull., 57*, 349-369, 1973.

Borgeld, J.C., J.A. Goff, L.A. Mayer, and J.E. Hughes-Clarke, Surface character of the Eel River flood deposit on the shelf: Swath backscatter and surface sediments, *Mar. Geol., 154*, 197-210, 1999.

Buck, K.F., H.C. Olsen, and J.A. Austin, Jr., Paleoenvironmental evidence for latest Pleistocene sea-level fluctuations on the New Jersey outer continental shelf: Combining high resolution sequence stratigraphy and foraminiferal analysis, *Mar. Geol., 154*, 287-304, 1999.

Chave, A.D., Numerical integration of related Hankel transforms by quadrature and continued fraction expansion, *Geophysics, 48*, 1671-1686, 1983.

Chave, A.D., The Fréchet derivatives of electromagnetic induction, *J. Geophys. Res., 89*, 3373-3380, 1984.

Chave, A.D., and C.S. Cox, Controlled electromagnetic sources for measuring electrical conductivity beneath the oceans, 1, Forward problem and model study, *J. Geophys. Res., 87*, 5327-5338, 1982.

Chave, A.D., S.C. Constable, and R.N. Edwards, Electrical exploration methods for the seafloor, in *Electromagnetic Methods in Applied Geophysics*, Vol. 2, *Application*, edited by M. Nabighian, pp. 931-966 Soc. of Explor. Geophys., Tulsa, Okla., 1987.

Cheesman, S.J., R.N.Edwards, and A.D. Chave, On the theory of sea-floor conductivity mapping using transient electromagnetic systems, *Geophysics, 52*, 204-217, 1987.

Cheesman, S.J., L.K. Law, and B. St. Louis, A porosity survey in Hecate Strait using a seafloor electro-magnetic profiling system, *Mar. Geol., 110*, 245-256. 1993.

Clarke, S.H., Geology of the Eel River basin and adjacent region: Implications for late Cenozoic tectonics of the

southern Cascadia subduction zone and Mendocino triple junction, *AAPG Bull., 76*, 199-224, 1992.

Constable, S.C., Marine electromagnetic induction studies, *Surv. Geophys., 11*, 303-327, 1990.

Constable, S.C., R.L. Parker, and C.G. Constable, Occam's inversion: A practical algorithm for generating smooth models from electromagnetic sounding data, *Geophysics, 52*, 289-300, 1987.

Davies, T.A., and J.A. Austin, Jr., High-resolution 3D seismic reflection and coring techniques applied to late Quaternary deposits on the New Jersey shelf, *Mar. Geol., 143*, 137-149, 1997.

Davies, T.A., J.A. Austin, Jr., M.B. Lagoe, and J.D. Milliman, Late Quaternary sedimentation of New Jersey: New results using 3D seismic profiles and cores, *Mar. Geol., 108*, 323-343, 1992.

Duncan, C.S., J.A. Goff, J.A. Austin, and C.S. Fulthorpe, Tracking the last sealevel cycle: Seafloor morphology and shallow stratigraphy of the latest Quaternary New Jersey middle continental shelf, *Mar. Geol., 170*, 395-421, 2000.

Emery, K.O. and E. Uchupi, *The Geology of the Atlantic Ocean*, 1050 pp., Springer-Verlag, New York, 1984.

Evans, R.L., L. K. Law, B. St. Louis, S. Cheesman, and K. Sananikone, The shallow porosity structure of the Eel Shelf, northern California: Results of a towed electromagnetic survey, *Mar. Geol., 154*, 211-226, 1999.

Evans, R.L., L.K. Law, B. St. Louis, and S. Cheesman, Buried paleo-channels on the New Jersey continental margin: Channel porosity structures from electromagnetic surveying, *Mar. Geol., 170*, 381-394, 2000.

Field, M.E., J.V. Gardner, D.E. Drake and D.A. Cacchione, Tectonic morphology of offshore Eel River basin, California, in *Tectonics, Sedimentation and Evolution of the Eel River and Other Coastal Basins of Northern California*, edited by H. Schymiczek, and R. Suchsland, *San Joaquin Geol. Surv. Misc. Publ., 37*, 41-48, 1987.

Goff, J.A., D. Orange, L.A. Mayer, and J. Hughes-Clarke, Detailed investigation of continental shelf morphology from a high resolution swath sonar survey over the Eel River basin, northern California, *Mar. Geol., 154*, 255-269, 1999a.

Goff, J.A., D.J.P. Swift, C.S. Duncan, L.A. Mayer, and J. Hughes-Clarke, High resolution swath sonar investigation of sand ridge, dune and ribbon morphology in the offshore environment of the New Jersey margin, *Mar. Geol., 161*, 307-337, 1999b.

Goff, J.A., H.C. Olson, and C.S. Duncan, Correlation of sidescan backscatter intensity with grain size distribution of shelf sediments, New Jersey margin, *Geo Mar. Lett., 20*, 43-49, 2000.

Hughes-Clarke, J.E., The potential for seabed classification using backscatter from shallow water multibeam sonars: in *Acoustic Classification and Mapping of the Seafloor*, edited by N. Pace, and D.N. Langhorne, *Proc. Inst. Acoust., 15*, 381-388, 1993.

Hughes-Clarke, J.E., L.A. Mayer, and D.E. Wells, Shallow water imaging multibeam sonars: A new tool for investigating seafloor processes in the coastal zone and on the continental shelf, *Mar. Geophys. Res., 18*, 607-629, 1996.

Jackson, D.R., and K.B. Briggs, High-frequency bottom backscattering: Roughness versus volume scattering, *J. Acoust. Soc. Am., 92*, 962-977, 1992.

Jackson, P.D., D. Taylor-Smith, and P.N. Stanford, Resistivity-porosity-particle shape relationships for marine sands, *Geophysics, 43*, 1250-1268, 1978.

Kayen, R.E. and P. Thang, Using HyperCard for robotic control and data collection, *Scitech J., 7*, 24-29, 1997.

Kayen, R.E., B.D. Edwards, and H.J. Lee, Non-destructive laboratory measurement of geotechnical and geoacoustic properties through intact core-liner, in *Nondestructive and Automated Testing for Soil and Rock Properties*, edited by W.A. Marr, *Am. Soc. Test. Mater. (ASTM) Spec. Tech. Pub. STP-1350*, 83-94, 1999.

Lyons, A.P., and D.A. Abraham, Statistical characterization of high-frequency shallow water seafloor backscatter, *J. Acoust. Soc. Am., 106*, 1307-1315, 1999.

Mayer, L.A., J.E. Hughes-Clarke, J.A. Goff, C.L. Schuur, and D.J.P. Swift, Multibeam sonar bathymetry and imagery from the New Jersey continental margin; preliminary results, *Eos Trans. AGU, 77(46)*, Fall Meet. Suppl., 329, 1996.

Milliman, J.D., Z. Jiezao, L. Anchun, and J.I. Ewing, Late Quaternary sedimentation on the outer and middle New Jersey continental shelf: Result of two local deglaciations, *J. Geol., 98*, 966-976, 1990.

Mourad, P.D., and D.R. Jackson, High frequency sonar equation models for bottom backscatter and forward loss, in *Proceedings, OCEANS '89,* pp. 1168-1175, *IEEE Press,* Piscataway, N.J., 1989.

Nittrouer, C.A., STRATAFORM: Overview of its design and synthesis of its results, *Mar. Geol., 154*, 3-12, 1999.

Nittrouer, C.A., and J. H. Kravitz, STRATAFORM: A program to study the creation and interpretation of sedimentary strata on continental margins, *Oceanography, 9*, 146-152, 1996.

Smith, J.D., Geomorphology of a sand ridge, *J. Geol., 77*, 39-55, 1969.

Sommerfield, C.K., and C.A. Nittrouer, Modern accumulation rates and a sediment budget for the Eel shelf: A flood-dominated depositional environment, *Mar. Geol., 154*, 227-241, 1999.

Swift, J.P., G. Parker, N.W. Lanfredi, G. Perillo, and K. Figge, Shoreface-connected sand ridges on American and European shelves: A comparison, *Estuarine Coastal Mar. Sci., 7*, 257-273, 1978.

Wheatcroft, R.A., C.K. Sommerfield, D.E. Drake, J.C. Borgeld, and C.A. Nittrouer, Rapid and widespread dispersal of flood sediment on the northern California continental margin, *Geology, 25*, 163-166, 1997.

Wong, P., J. Koplik, and J.P. Tomanic, Conductivity and permeability of rocks, *Phys. Rev. B., Condens. Matter, 30*, 6606-6614, 1984.

R. L. Evans, Department of Geology and Geophysics, Woods Hole Oceanographic Institution, Clark South 172, Woods Hole, MA 02543, USA. (revans@whoi.edu)

(Received June 12, 2000; revised July 2, 2001; accepted July 3, 2001.)